Geometric Morphometric Assessment of Sexually Dimorphic Characteristics of the Distal Humerus

V.L. Vance[a,b], M. Steyn[a]

[a] *Forensic Anthropology Research Centre, Department of Anatomy, University of Pretoria, Pretoria, South Africa*

[b] *Oregon State Police Portland Metro Forensic Laboratory, 13309 SE 84th Avenue Suite 200, Clackamas, Oregon, 97015 U.S.A.*

Running title: Geometric morphometrics of the distal humerus

Corresponding author:
Prof. M Steyn, PhD, Department of Anatomy, University of Pretoria, Private Bag X323, Arcadia, 0007
South Africa
e-mail: maryna.steyn@up.ac.za
Fax: +27-866986463
Tel: +27-12-4203256; +27-82-8861719

Abstract

A number of recent studies investigated the use of morphological characteristics of the distal humerus to estimate the sex of unknown individuals. Using visual assessment, accuracies ranging from 74% to more than 90% were reported. The aim of this study was to assess these traits with geometric morphometrics, in order to determine if they corroborate the findings as described with pure visual assessment. A total sample of 155 female and 175 male humeri of South Africans were used. All humeri were photographed in standardized positions from a posterior and inferior view, and homologous landmarks assigned. Olecranon fossa shape, angle of the medial epicondyle and trochlear symmetry were assessed. Males and females could be separated with accuracies ranging from 78 – 91%. The results of this study confirm the existence of these traits and their usability in assessment of sex from skeletal remains, and the observed anatomical characteristics largely agree with what have been described by visual assessment.

KEY WORDS forensic anthropology, sex determination, distal humerus, sexual dimorphism, South Africa, olecranon fossa shape, trochlear symmetry

Introduction

Forensic anthropologists depend on the sexually dimorphic characteristics of the cranial and post-cranial skeleton to determine the sex of unknown remains. These characteristic physical differences expressed between males and females can manifest as either size or shape differences, and have been assessed and described in many of the bones of the human skeleton. Several studies where the humerus is used in an attempt to estimate sex have been published. Many of these studies have focused on size differences alone (e.g., Steyn and İşcan, 1999; Albanese et al., 2005; Frutos, 2005), with generally good results producing accuracies that are frequently above 80%. Morphological differences of both the distal and proximal humerus have also been studied, but to a lesser extent (Rogers, 1999; Rogers, 2009; Kranioti et al., 2009; Vance et al., 2011). Specifically the distal humerus is known to be dimorphic, and this is said to be due to differences in the carrying angle of the articulated humerus, radius and ulna (Grabiner, 1989; Fuss, 1991; Kingston, 2000). The increased lateral deviation of the forearm relative to the axis of the upper arm distinguishes females from males. This angle is said to be about 10 to 15 degrees in males and 20 to 25 degrees in females (Rogers, 1999).

These differences in the carrying angles between males and females are thought to be the reason why there are several macroscopically observable differences between the sexes in the distal humerus. Rogers (1999) described four characteristics which she used to develop a new method of determining sex, with average accuracies ranging from 74 to 91%. When using a combination of characteristics, accuracies of up to 94% were obtained. These sexually dimorphic differences were found in olecranon fossa shape (triangular in males, oval in females), angle of the medial epicondyle (extends parallel to horizontal surface in males when placed posterior side upwards; angles upwards in females), trochlear symmetry (medial edge of trochlea extends further than the lateral edge in males; in females they are more equal in shape) and trochlear constriction (constricted and bow-tie shaped in females, less so in males). These findings were corroborated by Falys et al. (2005). Rogers (2009) then used the same methods to assign sex to juvenile and adolescent humeri, and found 80% accuracy in males and 82% accuracy in females.

Vance et al. (2011) used a large sample of 608 individuals from South Africa (420 males, 188 females) to test the accuracy of this method. They found it difficult to score trochlear constriction consistently, and discarded it from the list of characteristics because it gave

confusing results. Using a scoring system where the aggregate score of the remaining three features were assessed, accuracy rates of 77% for females and 74% for males were found. This classification rate is lower than what was found in previous studies, but suggests that characteristics of the distal humerus are valuable when estimating skeletal sex.

The practice of using morphological characteristics to assess sexual dimorphism can be criticized, because there is some subjectivity involved (Pretorius et al., 2006; Kranioti et al., 2009). It is very difficult to consistently assign a score to a specific feature, and the accuracy may be dependent on the experience of the observer. It is also difficult to analyse results of these types of studies statistically. Geometric morphometrics have been used extenisvely in the last few years to quantify morphological characteristics (Kendall, 1981, 1984; Bookstein, 1989, 1991, 1996; Rohlf & Slice, 1990; Rohlf & Marcus, 1993; Slice, 1993; Rohlf, 1998; Rohlf, 2003), and have been shown to be a very useful tool in assessing shape variations in the human skeleton (Hennessy and Stringer, 2002; Pretorius et al., 2006; Kranioti et al., 2009). It allows for a detailed assessment of various aspects that may contribute towards differences in shape, and can also quantify the accuracies with which skeletons can be sorted into various groupings (e.g., sex) based on the observed shape differences. Two- and three-dimensional geometric morphometric assessments have been used to study sexual dimorphism in, for example, the skull (Rosas & Bastir, 2002; Bigoni et al., 2010), mandible (Oettlé et al., 2005; Franklin et al., 2007; Franklin et al., 2008), pelvis (Steyn et al., 2004; Gonzalez et al., 2009); and scapula (Scholtz et al., 2010).

Kranioti et al. (2009) also used geometric morphometrics to study shape differences in the proximal and distal ends of the humerus. In females, the greater tubercle of the humerus was found to be smoother, with a less pronounced superior border. According to these authors females also have a relatively squared distal epiphysis, whereas those of males are more rectangular (being wider in general). Males tend to have more voluminous distal epiphyses, with relatively wider lateral trochleas and smaller capitula.

The aim of this study was to use geometric morphometrics to verify the existence of the observed shape differences in the distal humerus in order to assess whether the shape differences observed with the naked eye can also be quantified in an independent manner. It will also be determined to what degree of accuracy geometric morphometric assessment is able to separate males and females using these characteristics.

Materials and methods

The skeletal sample in this study originated from the Pretoria Bone Collection at the Department of Anatomy, University of Pretoria (L'Abbé et al., 2005) and the Raymond Dart Collection at the University of Witwatersrand (Dayal et al., 2009). All individuals are known, and their ages ranged between 19 and 94 years (male mean age 56 years, females 53 years). A total of 138 South African whites (55 female, 66 male) and 208 South African blacks (100 female, 108 male) were used, to ensure that all possible variation is included.

Standardized landmarks were chosen for two 2-dimensional views of the distal humerus for geometric morphometric analyses. The first view gave a perspective of the distal and inferior humerus which documented the angle of the medial epicondyle (referred to as the "EPI" view, Fig. 1). The second view was of the posterior side of the humerus which documented the olecranon fossa shape and trochlear extension (referred to as the "OL" view, Fig. 2). The first (EPI) view thus reflected the angle of the medial epicondyle, but also included the inferior view of the trochlea. The second view (OL) combined both the shape of the olecranon fossa and the trochlear symmetry, corresponding to the features as described by Vance et al. (2011).

Each humerus was positioned in a standardized manner, and a digital image taken. For the EPI view of the humerus, the left humerus was placed on grid paper on an osteometric board with the posterior side facing upwards. The superior surface of the humeral head and greater tubercle touched the upper left-hand-corners of the osteometric board. The distal end of the humerus was then aligned along a grid paper axis to place the trochlear constriction (the indentation made between the capitulum and the trochlea) in a standardized location, 11 centimetres to the right of the left margin of the osteometric board. This was done to eliminate the variation of curvature that exists in this element (which was not an important characteristic to capture). The camera lens was at a perpendicular angle to the bone surface.

Photographs were taken of the inferior "spool" feature of the distal humerus with a Cannon SureShot 95 digital camera. The camera was placed in a fixed position on a tripod 30 cm from the surface of the bone, in front of the inferior feature. A reference number corresponding to the specimen number was placed in the image for consistency in image file maintenance. The viewfinder was focused on the middle of the bone and this allowed for all humerii to exhibit the feature within the frame. The captured images were saved and recorded with reference numbers

onto a computer, and 19 homologous landmarks were assigned with tpsDig for geometric morphometric analysis (Table 1; Figure 1).

For the OL view of the humerus, each bone was placed on graph paper on an osteometric board with the posterior side facing upwards. The superior surface of the humeral head and greater tubercle touched the upper left-hand-corners of the osteometric board, as in the EPI perspective. The distal end of the humerus was then aligned along a grid paper axis to place the trochlear constriction in a standardized location, 11 centimetres to the right of the left margin of the osteometric board. This ensured that the inferior edges of the trochlea and capitulum were correctly aligned with each other.

Images were captured with the camera mounted on a small tripod 30 centimetres above the surface of the bone, corresponding to the grid paper axis. In doing so, the feature was exhibited within the frame of the photograph. A reference number corresponding to the specimen number was placed in the image for consistency in image file maintenance. The captured images were entered into a computer and 15 landmarks were assigned to each humerus to use for geometric morphometric analysis (Table 2; Fig 2).

The entire dataset for each view was divided first into male and female subgroups, after which they were divided into black and white subsets. Generalized least-squares Procrustes analysis was used to compute the average shape for each sample (Hennessy and Stringer, 2002; Rohlf, 2000; Loy et al., 1999). Landmarks were then used to perform geometric morphometric analyses on each of the two perspectives in a series of steps, based on the tps program tpsDig, (FJ Rohlf, Version 1.31), tpsSplin (FJ Rohlf, Version 1.14), tpsRelw (FJ Rohlf, Version 1.25), as well as the IMP package (Integrated Morphometrics Package) specifically CoordGen, CVAGen6 and TwoGroup (Bookstein, 1990; Slice et al., 1998; Sheets, 2001; Rohlf, 2000; Bookstein et al., 2003; Rohlf, 2003; Slice et al., 2009).

TpsSplin was used to compare the same homologous landmarks in different specimens by utilizing thin-plate spline transformations. A preliminary reference shape is produced which is the average shape of the entire sample population, and is designated by a precise perpendicular grid pattern exhibiting no deformations of 90-degree angles with the homologous landmarks included. The thin-plate splines for each specimen illustrate the deformation (or incongruence) of this grid. Deformation grids of the consensus configurations of the groups made it possible to determine where the variation was for each perspective. The consensus thin-plate splines were

also viewed in "vector mode" to determine which landmarks were responsible for the greatest amount of variation. In other words, vector thin-plate splines indicate where and by how much the landmarks of two specimens in the sample group differ from each other.

Differences in shape were determined and analyzed using tpsRelw. This shows the distribution of specimens within the groups that are to be compared to each other in order to scrutinize intra-sample distinctions. This is presented in graph form to make the representation of any variation between groups in a sample population possible to visualize.

Statistically significant differences between groups were assessed by means of discriminant function analysis (or CVA) using CVAGen6. A Canonical Variates Analysis assesses the ability to correctly classify random, individual specimens in a dataset to groups (e.g. male or female). This determines the predictive ability of a certain morphological feature. Goodall's F-test was used to calculate p-values to determine the statistical significance, if any, of the separation of the morphological feature analyzed. Goodall's F-test specifically compares the Procrustes distance between the means of two samples to the amount of variation found in the samples.

To test for inter-and intra-observer repeatability, 15 male and 15 female specimens were randomly selected and re-assigned the homologous landmarks for each of the views of the distal humerus. This was done by the primary observer and an independent observer. This repeated landmark data were statistically compared to the original data set using Hotelling's T^2 –test and Goodall's F-test of the TwoGroup programme. No statistically significant differences between the shapes were found for the inter- or intra-observer sets of data.

Results

The differences between males and females in EPI view were significant at $p<0.001$, also when separated into ancestral groups. The consensus thin plate splines for all males and females in the EPI view are shown in Fig 3. Fig 4 shows the consensus thin plate splines in vector mode, specifically the difference between the females (circles) and the males (arrows). This clearly shows the trend for female epicondyles to be angled upwards, whereas the male epicondyle tends to be more horizontal. This is especially observable in landmarks 9 – 12. These differences were also statistically significant at $p<0.001$ with all males and females combined, and when they were separated into ancestral groups.

Table 3 shows the accuracy with which all humeri were separated into males and females. With all groups combined, the accuracy was 79% for females and 78% for males. This improved to 83% and 85% respectively when only the black individuals were assessed, and 91% and 90% for the whites. The differences between ancestral groups are also demonstrated by the consensus relative warp analysis (Fig. 5), where some separation between the four groups can be seen. In OL view, males and female shapes differed significantly ($p<0.001$) for all groups combined and also when divided into black and white groups. The consensus thin plate spline for the OL view is shown in Fig. 6. This OL view reflects both the olecranon fossa shape and the trochlear symmetry/asymmetry. Fig 7 shows the male-on-female difference in vector mode. The more triangular shape of the olecranon fossa in males is illustrated in the upward displacement of landmarks 5 and 6 and the lower positioning of landmark 4. The male trochlea ia also more assymetrical with both the medial epicondyle (landmark 12) and medial edge of the trochlea (landmark 15) being situated relatively lower in relation to the lateral side (landmarks 1 and 11). These differences were statistically significant (all features in OL view combined), with all p-values less than 0.001.

Table 6 shows the accuracy with which the posterior humeri were separated into males and females. Accuracies of 83% and 84% were achieved for groups combined, or 81 – 88% when the groups were separated (Tables 7 & 8). The concensus relative warp analysis is shown in Fig. 8.

Discussion

Although size-based methods using multiple discriminant analysis or other statistical models such as logistic regression are generally easier to use in determination of sex than morphological methods (e.g., Albanese, 2003; Albanese et al., 2005;), it has been shown that considerable variation exists in robusticity of the distal humerus in South Africans (Steyn & Iscan, 1999). Morphological assessment can therefore strengthen the diagnosis of sex, and can also be of use in cases where the bone is damaged such that measurements are not possible.

In general, the EPI view (which depicted the angle of the medial epicondyle of the distal humerus) provided a unique and quantifiable way in which to accurately designate sex. The sexual dimorphism of the element was clearly visible in the vector modes of the thin plate splines, confirming what is seen with the naked eye. In the consensus relative warp analysis (Fig. 5), males and females were seen at quite a distance from each other in this perspective.

Statistical analysis indicated that90.5% of the white group (on average) was accurately separated, whereas the figure for the black group is 84%. This may suggest that all groups are not equally sexually dimorphic, but as Albanese & Saunders (2006) point out, these differences are more likely to be due to mortality bias, secular trend, collection bias or differences in sampling. However, males were always seen quite separate from their female equivalents and exhibited features of the medial epicondylar angle that were also observed in visual assessment by previous researchers.

The medial epicondyle itself exhibited the most pronounced differences between males and females, which was expected. When the medial epicondyle sits more centrally within the profile of the trochlea, there was more trochlear surface area surrounding the medial epicondyle. This, in turn, positioned the entire medial epicondyle further into an anterior position, thus closer to the tabletop on which the bone actually rested. This was the pattern most commonly seen in males. The amount of trochlear area between the posterior and anterior portion of the medial epicondyle allowed the male trochlea to project directly outward, parallel to the tabletop. With the lack of posterior surface area in the female trochlea surrounding the medial epicondyle, there was more possibility to angle away from the tabletop based on less physical bone for ligament and tendon insertion. The female medial epicondyle, in turn, appeared more elevated along the surface of the bone and provided for a large amount of deviation between the male and female form. These skeletal features most probably correspond to soft tissue features that act upon the distal humerus, and these medial epicondylar angle differences were thought to be directly related to 1) the carrying angle of the arm, 2) where the ulnar collateral ligament actually originates on the female medial epicondyle as opposed to the male epicondyle, and 3) how this difference in tension, torsion, extension and flexion would affect the hard tissue anatomy of the elbow joint. This joint has been proven to be sexually dimorphic (Grabiner, 1989) and thus the variation between males and females in this particular element can also be seen in hard tissue morphology.

Olecranon fossa shape and trochlear extension were also considered accurate predictors of sex when non-metric visual analysis was performed on each in isolation (Vance et al., 2011). Analysis of the OL perspective in the current study confirmed their usability in separating males from females, with an average accuracy rate of 83.5%. The most important feature to observe when viewing the olecranon fossa shape is the upward projection of the fossa towards the shaft,

producing a superior "point" at the apex of the fossa. This made the fossa appear more triangular, which was considered a classic male trait. As seen in Figure 7 this point is located more superiorly in males (the arrow of landmark 5) than in females (the point). In addition, trochlear extension clarifies male from female morphology by positioning the inferior margin of the trochlea farther downward (inferiorly) to that of females, which would form the visual equivalent of "extension" in this region (landmark 15 in Fig. 7). Again, the morphology of the olecranon fossa and the trochlea most probably correspond to soft tissue features that act upon the distal humerus. These include the junction of the humerus to the ulna, which forms an articular surface between the two as described by Fuss (1991). Grabiner (1989) also documented the articulation between the distal humerus and the ulna within the olecranon fossa, and saw differences between males and females in the carrying angle of the arm at this location. Thus the variation between males and females in this particular element can also be seen in hard tissue morphology.

Males and females were classified with high levels of accuracy (>80%) with geometric morphometrics, and morphometrics could categorize males and females from each other more accurately than visual techniques (74 - 77%, Vance et al 2011). Traits of the distal humerus are thus very usable in the estimation of sex, and what is seen on a macroscopic level was confirmed in this study by using geometric morphometrics. This also agrees in general with what was found by Kranioti et al. (2009), although they found the most pronounced differences in the distal humerus to be related to a wider distal epiphysis and relatively smaller capitulum in males. These were not specifically assessed in the current study.

Conclusion

Clear differences between male and female distal humeri could be observed when viewed from the back and inferiorly. Using geometric morphometric analysis, humeri could be separated with high levels of accuracy which are comparable to those observed for previous metric and non-metric studies of the humerus. This skeletal element can thus be deemed sexually dimorphic, and geometric morphometrics mostly increased the classification accuracy by observing differences in form that the naked eye may not have seen.

Acknowledgements

The authors would like to thank Y Scholtz and E Pretorius for help with the geometric morphometric analyses, and M Pretorius for assistance with the figures. We are grateful for the use of the Pretoria Bone Collection. The first author also offers sincere thanks to the Oregon State Police Forensics Division for their support of these studies. The research of M Steyn is funded by the National Research Foundation of South Africa (NRF). Any opinions, findings and conclusions or recommendations expressed in the material are those of the authors and therefore the NRF do not accept any liability in regard thereto.

References

Albanese, J., 2003. A metric method for sex determination using the hipbone and femur. J. Forensic Sci. 48, 263-273.

Albanese, J., Cardoso, H.F.V., Saunders, S.R., 2005. Universal methodology for developing univariate sample-specific sex determination methods: an example using the epicondylar breadth of the humerus. J. Archaeol. Sci. 32, 143-152.

Albanese, J., Saunders, S.R., 2006. Is it possible to escape racial typology in forensic indentification? In: Schmitt, A., Cunha, E., Pinheiro, J. (Eds.) Forensic Anthropology and Medicine – Complementary Sciences from Recovery to Cause of Death. Humana Press, New Jersey, pp.281-316.

Bigoni, L., Velemínská, J., Brůžek, J., 2010. Three-dimensional geometric morphometric analysis of cranio-facial sexual dimorphism in a Central European sample of known sex. HOMO – J. Comp. Hum. Biol., 61, 16-32.

Bookstein, F.L., 1989. Size and shape: a comment on semantics. Syst. Zool. 38, 173-180.

Bookstein, F.L., 1990. Introduction to methods for landmark data. In: Rohlf, F.J., Bookstein, F.L. (Eds.) Proceedings of the Michigan Morphometrics Workshop, 1988 May 16–28, Ann Arbor, Michigan. University of Michigan Museum of Zoology, Ann. Arbor., pp. 215–225.

Bookstein, F.L., 1991. Morphometric Tools for Landmark Data: Geometry and Biology. Cambridge University Press, Cambridge.

Bookstein, F.L., 1996. Combining the tools of geometric morphometrics. In: Marcus, L.F., Corti, M., Loy, A., Naylor, G.J.P., Slice, D.E. (Eds.) Advances in Morphometrics. Plenum Press, New York, pp. 131-151.

Bookstein, F.L., Gunz, P., Mitteroecker, P., Prossinger, H., Schæfer, K., Seidler, H., 2003. Cranial integration in Homo: singular warps analysis of the midsagittal plane in ontogeny and evolution. J. Hum. Evol. 44, 167–187.

Dayal, M.R., Kegley, A.D.T., Strkalj, G., Bidmos, M.A., Kuykendall, K.L., 2009. The history and composition of the Raymond A. Dart Collection of human skeletons at the University of the Witwatersrand, Johannesburg, South Africa. Am. J. Phys. Anthropol. 140, 324-335.

Falys, C.G., Schutkowski, H., Weston, D.A., 2005. The distal humerus: a blind test of Rogers' sexing technique using a documented skeletal collection. J. Forensic Sci. 50, 1289-1293.

Franklin, D., Oxnard, C.E., O'Higgins, P., Dadour, I., 2007. Sexual dimorphism in the subadult mandible: quantification using geometric morphometrics. J. Forensic Sci. 52, 6-10.

Franklin, D., O'Higgins, P., Oxnard, C.E., 2008. Sexual dimorphism in the mandible of indigenous South Africans: a geometric morphometric approach. South Afr. J. Sci. 104, 101-106.

Frutos, L., 2005. Metric determination of sex from the humerus in a Guatemalan forensic sample. Forensic Sci. Int. 147, 153-157.

Fuss, F.K., 1991. The ulnar collateral ligament of the human elbow joint. J. Anat. 175, 203-212.

González, P.N., Bernal, V., Perez, S.I., 2009. Geometric morphometric approach to sex estimation of human pelvis. Forensic Sci. Int. 189, 68-74.

Grabiner, M.D., 1989. The elbow and radioulnar joints. Lea and Febiger, London.

Hennessy, R.J., Stringer, C.B., 2002. Geometric morphometric study of the regional variation of modern human craniofacial form. Am. J. Phys. Anthropol. 117, 37-48.

Kendall, D.G., 1981. The statistics of shape. In: Barnett V, editor. Interpreting Multivariate Data. Wiley, New York, pp. 75-80.

Kendall, D.G., 1984. Shape manifolds, procrustean metrics and complex projective spaces. Bull. London Math. Soc. 16, 81-121.

Kingston, B., 2000. Understanding Joints: A Practical Guide to Their Structure and Function. United Kingdom: Stanley Thornes Ltd.

Kranioti, E.F., Bastir, M., Sánchez-Meseguer, A., Rosas, A., 2009. A geometric morphometric study of the Cretan humerus for sex identification. Forensic Sci. Int. 189, 111.e1-8.

L'Abbé, E.N., Loots, M., Meiring, J.H., 2005. The Pretoria Bone Collection: a modern South African skeletal sample. HOMO – J. Comp. Hum. Biol. 56, 197-205.

Loy, A., Boglion, C., Cataudella, S., 1999. Geometric morphometrics and morpho-anatomy: a combined tool in the study of sea bream (Sparus aurata, sparidae) shape. J. Appl. Icthyol. 15, 110.

Oettlé, A.C., Pretorius, E., Steyn, M., 2005. Geometric morphometric analysis of mandibular ramus flexure. Am. J. Phys. Anthropol. 128, 623-629.

Pretorius, E., Steyn, M., Scholtz, Y., 2006. Investigation into the usability of geometric morphometric analysis in assessment of sexual dimorphism. Am. J. Phys. Anthropol. 129, 64-70.

Rogers, T.L., 1999. A visual method of determining the sex of skeletal remains using the distal humerus. J. Forensic Sci. 44, 57-60.

Rogers, T.L., 2009. Sex determination of adolescent skeletons using the distal humerus. Am. J. Phys. Anthropol. 140, 143-148.

Rohlf, F.J., 1998. On applications of geometric morphometrics to studies of ontogeny and phylogeny. Syst. Biol. 47, 147-158.

Rohlf, F.J., 2000. Statistical power comparisons among alternative morphometric methods. Am. J. Phys. Anthropol. 111, 463-478.

Rohlf, F.J., 2003. Bias and error in estimates of mean shape in geometric morphometrics. J. Hum. Evol. 44, 665-683.

Rohlf, F.J., Marcus, L.F., 1993. A revolution in morphometrics. Trends in Ecological Evol. 8, 129-132.

Rohlf, F.J., Slice, D., 1990. Extensions of the procrustes method for the optimal superimposition of landmarks. Syst. Zool. 39, 40-59.

Rosas, A., Bastir, M., 2002. Thin-plate spline analysis of allometry and sexual dimorphism in the human craniofacial complex. Am. J. Phys. Anthropol. 117, 236-245.

Scholtz, Y., Steyn, M., Pretorius, E., 2010. A geometric morphometric study into the sexual dimorphism of the human scapula. HOMO – J. Comp. Hum. Biol. 61, 253-270.

Sheets, D.H., 2001. IMP, Integrated Morphometrics Package. Available from: URL: http://www.canisius.edu/~sheets/morphsoft.html; Sheets, David

Slice, D., 1993. Extensions, Comparisons and Applications of Superimposition Methods for Morphometric Analysis. State University of New York, New York.

Slice, D.E., Bookstein, F.L., Marcus, L.F., Rohlf, F.J., 1998. A Glossary for Geometric Morphometrics (Part 2). Available from: http://life.bio.sunysb.edu/morph/glossary/gloss2.html.

Slice, D.E., Bookstein, F.L., Marcus, L.F., Rohlf, F.J., 2009. A Glossary for Geometric Morphometrics (Part 1). Available from: http://life.bio.sunysb.edu/morph/glossary/gloss1.html.

Steyn, M., İşcan, M.Y., 1999. Osteometric variation in the humerus: sexual dimorphism in South Africans. Forensic Sci. Int. 106, 77-85.

Steyn, M., Pretorius, E., Hutten, L., 2004. Geometric morphometric analysis of the greater sciatic notch in South Africans. HOMO – J. Comp. Hum. Biol. 54, 197-206.

Vance, V.L., Steyn, M., L'Abbé, E.N., 2011. Non-metric sex determination from the distal and posterior humerus in black and white South Africans. J. Forensic Sci. 56, 710-714.

Table 1. Landmarks on the EPI view of the humerus (Fig. 1)

Landmark	Definition
Landmark 1	The medial margin of the lateral epicondyle on the top ridge of bone that constitutes the posterior surface of the capitulum.
Landmark 2	Situated halfway between landmark 1 and landmark 3.
Landmark 3	The lowest portion of the posterior spool, which constituted the inferior margin of the olecranon fossa.
Landmark 4	Situated halfway between landmark 3 and landmark 5.
Landmark 5	The most superior point of the medial margin/ridge of the posterior trochlea.
Landmark 6	The superior "root" of the medial epicondyle; where the posterior edge of the medial epicondyle meets the vertical ridge of the trochlea.
Landmark 7	Situated halfway between landmark 6 and landmark 8.
Landmark 8	Situated halfway between landmark 7 and landmark 9.
Landmark 9	Situated halfway between landmark 8 and landmark 10.
Landmark 10	The most medial point on the medial epicondyle.
Landmark 11	Situated halfway between landmark 10 and landmark 12.
Landmark 12	Situated halfway between landmark 11 and landmark 13.
Landmark 13	Situated halfway between landmark 12 and landmark 14.
Landmark 14	The inferior "root" of the medial epicondyle; where the inferior edge of the medial epicondyle meets the vertical ridge of the trochlea.
Landmark 15	The inferior edge of the trochlea. This landmark was placed where the straight vertical edge of the trochlea becomes curved again.
Landmark 16	The most constricted point on the anterior trochlear "spool".
Landmark 17	The most constricted point on the anterior capitulum "spool".
Landmark 18	The inferior border of the capitulum. This landmark was placed on the point where the curved edge becomes a distinct ridge.
Landmark 19	The lateral-most point of the lateral epicondyle.

Table 2. Landmarks on the OL view of the humerus (Fig. 2)

Landmark	Definition
Landmark 1	Situated on the supra-orbital ridge, aligned with the superior margin of the olecranon fossa. The grid paper place underneath the bone was used to assist in assigning this landmark, based on a grid line's linear progression across the bone, which most accurately showed the positioning of the upper margin of the olecranon fossa.
Landmark 2	The medial ridge of the humerus, place on the supra-condylar ridge, aligned with the superior margin of the olecranon fossa.
Landmark 3	The most lateral point of the olecranon fossa seen on the posterior surface. This landmark was not place within the fossa itself, but on the lateral edge of the fossa.
Landmark 4	The most medial point of the olecranon fossa, also placed on the surface of the bone as opposed to within the fossa itself.
Landmark 5	The most superior point of the olecranon fossa.
Landmark 6	The inferior edge of the olecranon fossa, directly in the middle. This landmark was placed halfway between landmark 3 and 4, and was placed on the smooth bone "ridge" that begins there.
Landmark 7	Situated halfway between landmark 3 and landmark 5.
Landmark 8	Situated halfway between landmark 4 and landmark 5.
Landmark 9	Situated halfway between landmark 3 and landmark 6, on the smooth bone "ridge" that begins in this location.
Landmark 10	Situated halfway between landmark 4 and landmark 6, where the smooth edge of bone begins in this location.
Landmark 11	The most lateral edge of the lateral epicondyle.
Landmark 12	The most medial point on the medial epicondyle.
Landmark 13	The inferior edge of the capitulum, at the point of the bone where the curved edge becomes a distinct ridge.
Landmark 14	The most constricted point of the posterior trochlear "spool".
Landmark 15	The inferior edge of trochlea, at the junction where the straight ridge become curved.

Table 3. Percentage of males and females correctly assigned using canonical variates analysis, EPI perspective (N = 347)

Group	CVA assignment based on shape data, EPI			
	Correctly assigned	Incorrectly assigned	Percentage correctly assigned	Chi square value
Females (*n*=163)	129	34	79%	
Males (*n*=184)	143	41	78%	**148.185***

**** Significant, at 0.05 level***

Table 4. Percentage of black males and black females correctly assigned using canonical variates analysis, EPI perspective (N = 208)

Group	CVA assignment based on shape data, EPI			
	Correctly assigned	Incorrectly assigned	Percentage correctly assigned	Chi square value
Black females (*n*=100)	83	17	83%	
Black males (*n*=108)	92	16	85%	**110.017***

****Significant, at 0.05 level***

Table 5. Percentage of white males and white females correctly assigned using canonical variates analysis, EPI perspective (*N* = 139)

Group	CVA assignment based on shape data, EPI			
	Correctly assigned	Incorrectly assigned	Percentage correctly assigned	Chi square value
White females (*n*=63)	57	6	91%	
White males (*n*=76)	68	8	90%	**107.188***

****Significant, at 0.05 level***

Table 6. Percentage of males and females correctly assigned using canonical variates analysis, OL perspective ($N = 348$)

Group	CVA assignment based on shape data, OL			
	Correctly assigned	Incorrectly assigned	Percentage correctly assigned	Chi square value
Females (n=163)	135	28	83%	
Males (n=185)	156	29	84%	**211.344***

**** Significant, at 0.05 level***

Table 7. Percentage of black males and black females correctly assigned using canonical variates analysis, OL perspective ($N = 210$)

Group	CVA assignment based on shape data, OL			
	Correctly assigned	Incorrectly assigned	Percentage correctly assigned	Chi square value
Black females (n=100)	82	18	82%	
Black males (n=110)	89	21	81%	**123.551***

****Significant, at 0.05 level***

Table 8. Percentage of white males and white females correctly assigned using canonical variates analysis, OL perspective ($N = 138$)

Group	CVA assignment based on shape data, OL			
	Correctly assigned	Incorrectly assigned	Percentage correctly assigned	Chi square value
White females (n=63)	55	8	87%	
White males (n=75)	66	9	88%	**111.226***

****Significant, at 0.05 level***

Fig. 1. Homologous landmarks for the EPI view. See description of each landmark location in Table 1

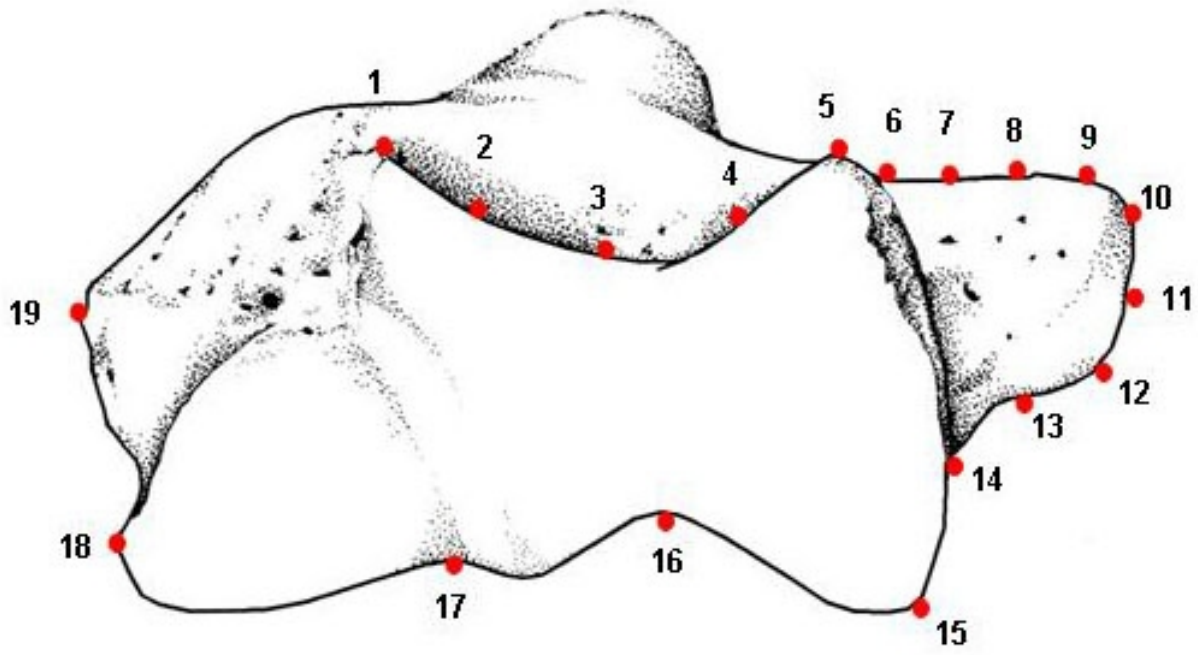

Fig. 2. Homologous landmarks for OL view. See description of each landmark in Table 2.

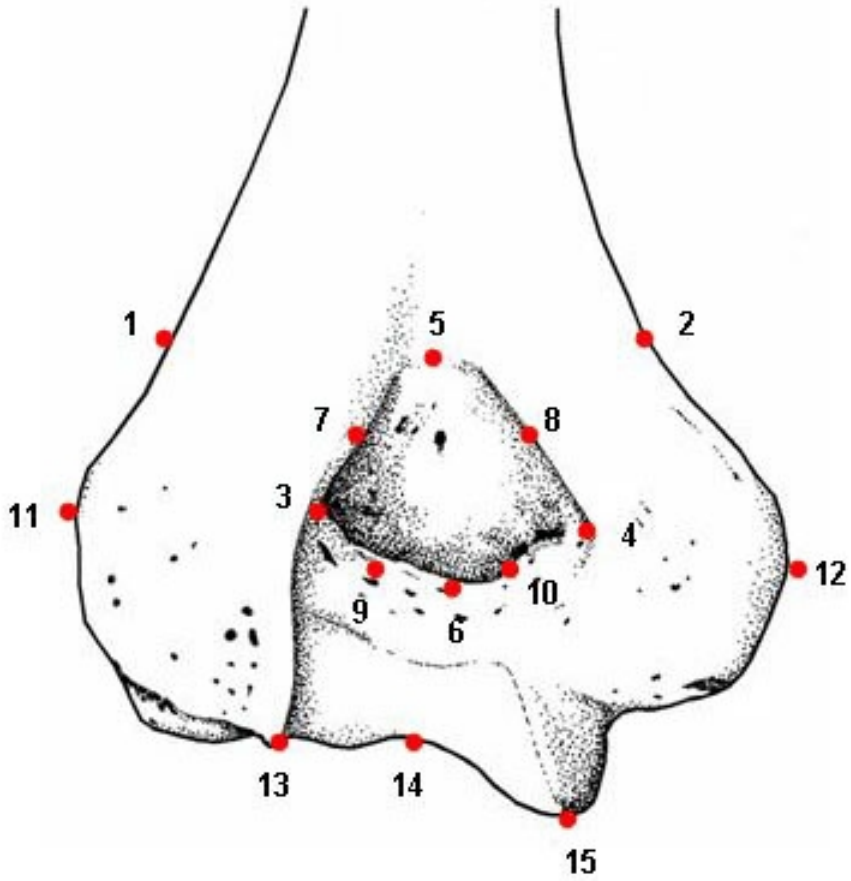

Fig. 3. Consensus thin-plate spline reference shape of all females and all males from the EPI perspective.

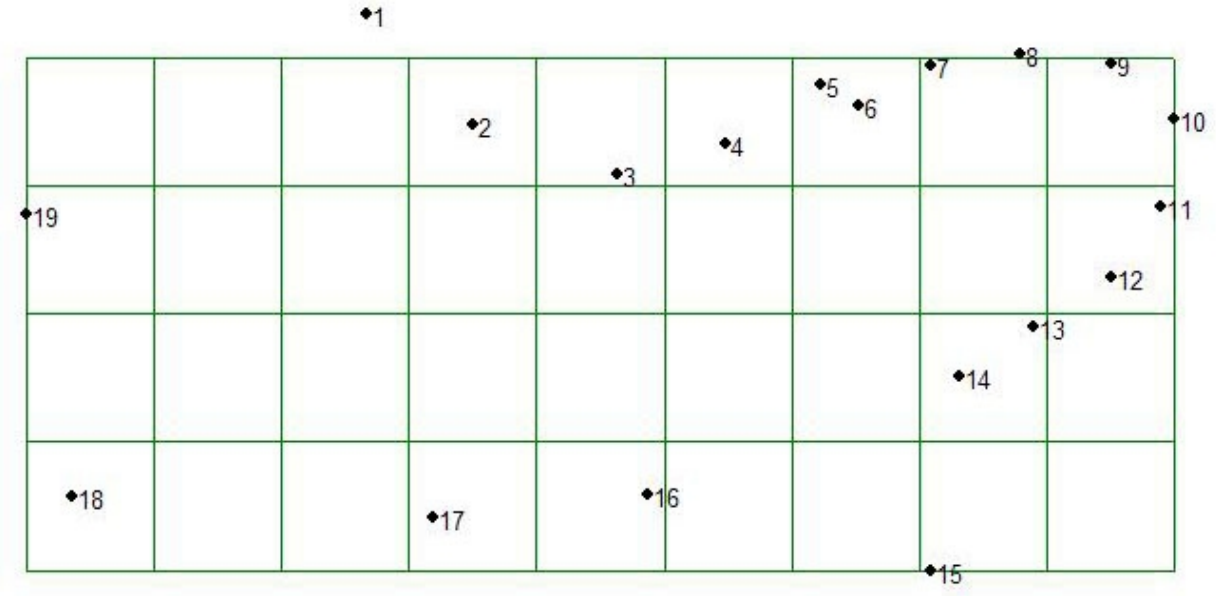

Fig. 4. Consensus thin-plate spline (in vector mode) demonstrating the differences between all females and all males, EPI perspective.

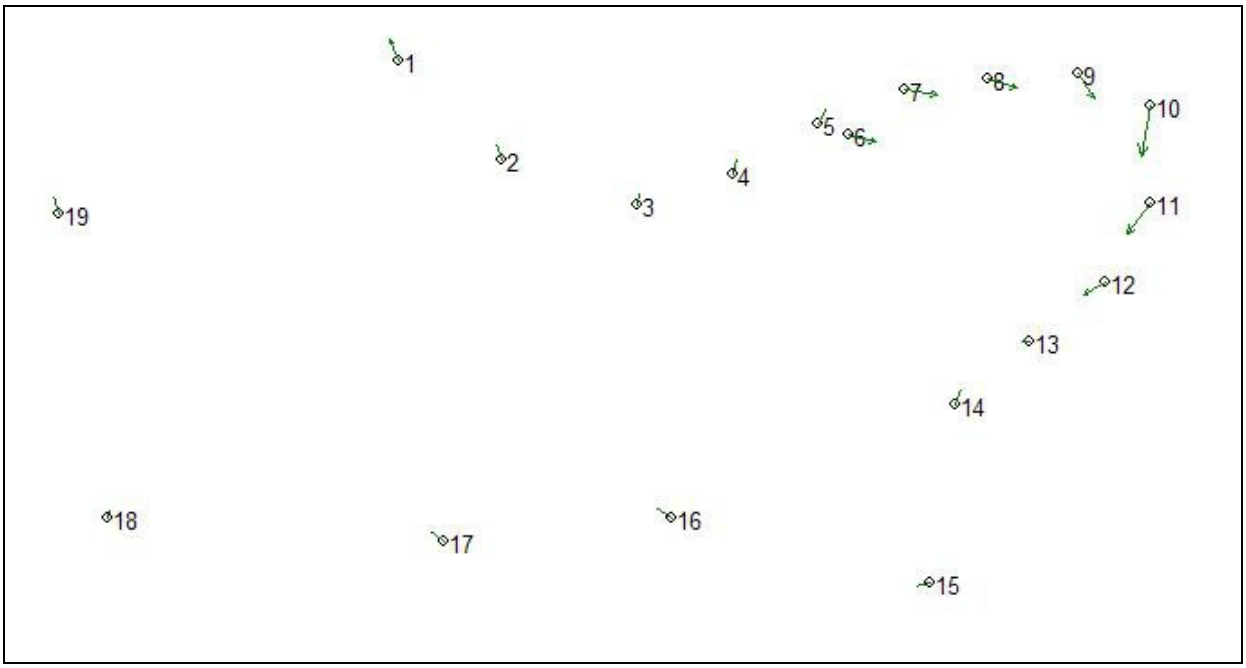

Fig. 5: Consensus relative warp analysis of females and males, EPI perspective.

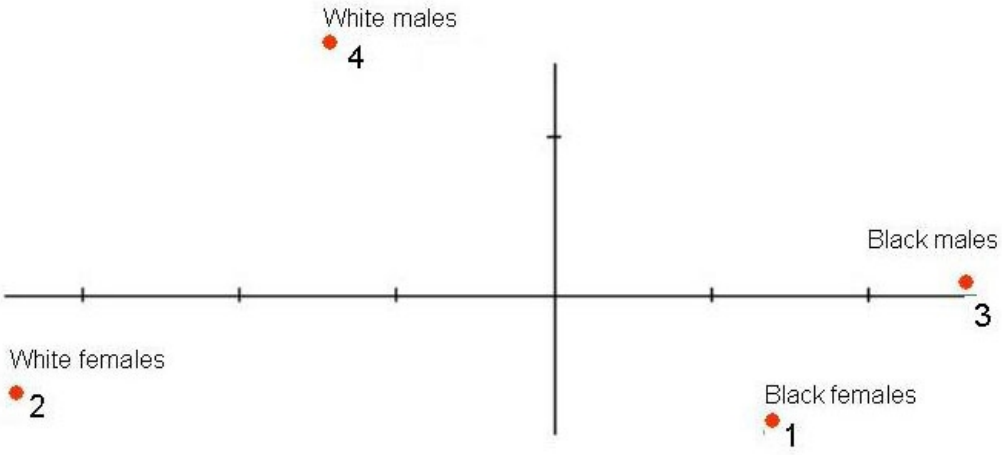

Fig. 6. Consensus thin-plate spline reference shape of all females and all males from the OL perspective.

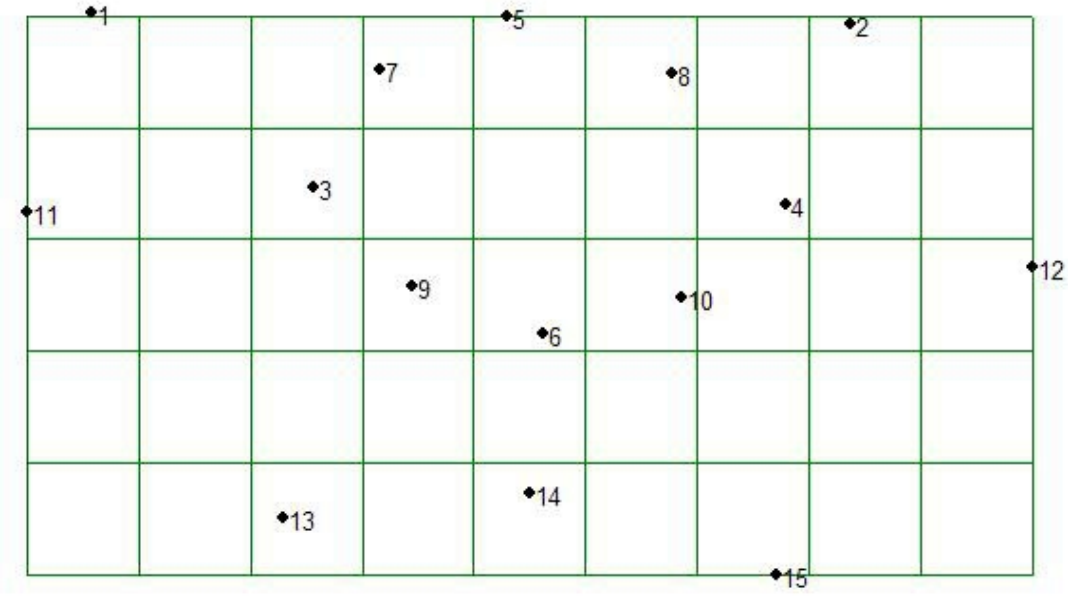

Fig. 7. Consensus thin-plate spline (in vector mode) demonstrating the differences between all females and all males, OL perspective.

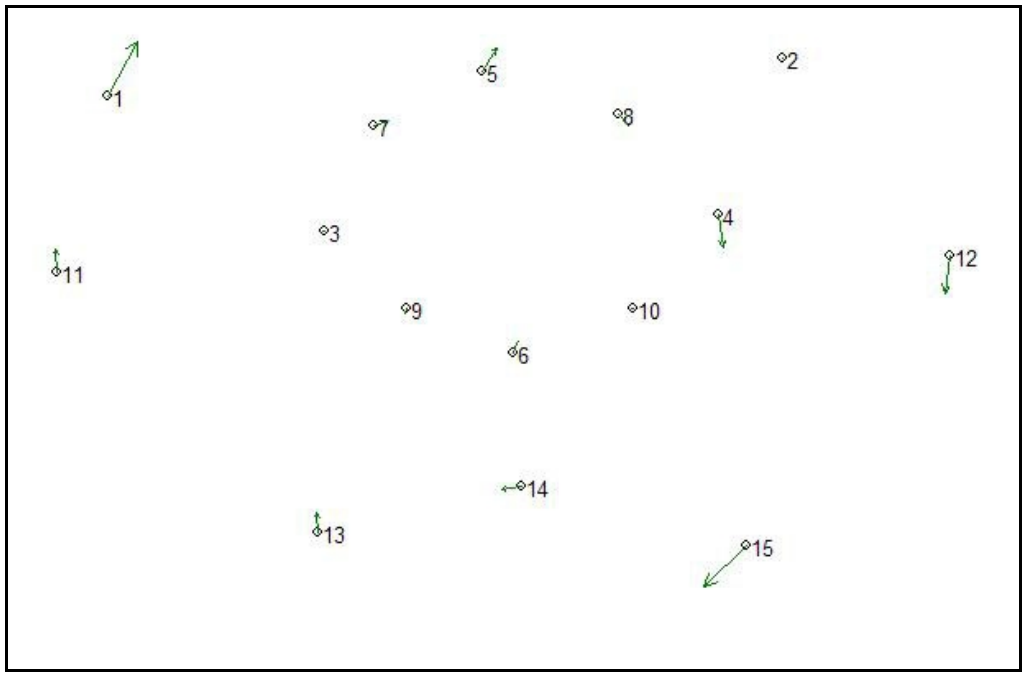

Fig. 8. Consensus relative warp analysis of females and males, OL perspective.